Hindawi
Advances in Civil Engineering
Volume 2023, Article ID 5983284, 16 pages
https://doi.org/10.1155/2023/5983284

Research Article

Application of BPNN Optimized by Fireworks Algorithm on Structural Bearing Capacity Analysis of Transmission Tower under Icing Conditions

Jian Guo [1] **and Wu Guo** [2]

[1]*College of Architecture and Civil Engineering, Qiqihar University, Qiqihar 161000, China*
[2]*College of Communication and Electronic Engineering, Qiqihar University, Qiqihar 161000, China*

Correspondence should be addressed to Jian Guo; 332923661@qq.com

Received 23 March 2023; Revised 9 July 2023; Accepted 17 July 2023; Published 31 July 2023

Academic Editor: Wei-yao Guo

With the increasing power demand in city development, the construction and application of transmission towers need to meet higher requirements. Icing is an extreme meteorological condition in the world, and icing disasters cause various accidents such as tower collapse and line disconnection of large-area lines every year. Therefore, it is of great significance to study the ultimate bearing capacity of transmission towers under icing conditions. The structural bearing capacity under icing is greatly affected by meteorological conditions and environmental factors, which has strong randomness and complexity, and brings a series of urgent problems to the structural stability of transmission towers. In the paper, the ultimate bearing capacity analysis and failure path research are conducted on the 500 kV linear cathead tower structure, and a structural bearing capacity prediction model based on the fireworks algorithm (FWA) is established. In order to accurately predict the structural bearing capacity, reduce the adverse effects of line icing, and ensure the structural stability of the transmission tower, the FWA is introduced into the neural network model. The self-adjusting mechanism of the local search ability and global search ability of the FWA is used to optimize the optimization process of weights and thresholds in the neural network, and a structural bearing capacity prediction model based on the FWA improved backpropagation neural network (BPNN) is proposed. Through the analysis and calculation of the measured data of the transmission tower in a certain area, and the comparative study with the traditional BPNN and the BPNN optimized by other common algorithms, the analysis and calculation results of the FWA-BPNN model used in this paper are closer to the actual value, the multiple indicators are more superior, and the model is more stable, which can realize the rapid and accurate analysis of the axial stress of tower members and maximum displacement between member nodes of the transmission tower under the icing condition.

1. Introduction

Social production and development cannot be separated from the support of power engineering construction. Power system is a large and complex lifeline system engineering, in which the transmission and transmission links are an indispensable part [1–3]. If there is a problem in the transmission link, it will lead to the normal operation of the entire power supply system, which will have a serious impact on the normal production and living order of the people. At the same time, it will have very serious consequences for the stable and sustainable development of society, resulting in immeasurable economic losses. Therefore, it is particularly important to study the ability of transmission tower line system to prevent major natural disasters. Moreover, with the increasing demand for electricity, the level and scale of transmission lines also need to be upgraded, which means that the span and height of transmission lines will increase with the increase of demand [4]. Meanwhile, the engineering technology problem is that the long-span high-voltage transmission tower line system structure will cause more serious damage under the action of icing and other loads, resulting in a threat to the safety of people's lives and property [5]. Similarly, under meteorological disasters, the damage of transmission lines is more significant.

Transmission tower line system structure is a kind of spatial steel structure with large overall span and high and flexible structure. It is a complex coupling structure system formed by the transmission tower as the spatial support part and the transmission tower erecting the conductor line through insulators and other hardware, so it is extremely sensitive to lateral loads [6]. Compared with other high-rise building structures, the dynamic response of transmission tower line system under external force load is very complex due to its own tower line coupling effect [7]. Therefore, when studying the overall structure of transmission tower line system, the transmission tower structure cannot be studied alone, and the influence of transmission lines should be considered at the same time. By means of theoretical analysis and field measured data comparison and verification, the establishment of a reasonable and sufficiently accurate transmission tower line system bearing capacity prediction model and dynamic calculation method is the basis for the study of transmission tower line system structure. Moreover, it can also provide corresponding reference for the study of other high flexible and complex space coupled steel structure systems and other attached suspension structures.

Icing is an extreme meteorological condition, which causes accidents such as line tripping, line breaking, tower toppling, conductor galloping, insulator flashover, and communication interruption in a large area all over the world every year [8]. Power grid safety accidents due to icing disasters have happened in Canada, Russia, the United States, Japan, Finland, Britain, Iceland, and China, causing huge economic losses. Since the 1940s, icing disaster has become a concern of academic and engineering field in many countries all over the world.

Transmission tower line system is the main body of transmission lines and the main carrier of long-distance power transmission. The damage caused by icing to the transmission tower line system is largely due to the excessive thickness of icing, which causes the stress of conductors, fittings, insulators, and towers to exceed their ultimate strength, or the tower collapse accident caused by the uneven icing of adjacent spans of the transmission tower and the unbalanced tension caused by deicing at different stages [9]. Because the weight of transmission tower is usually large, the foundation subsidence and foundation burst caused by tower collapse also occur from time to time. In addition, the tower falling and line breaking accident in the first gear will exert an unbalanced force on the other gear, and when it is serious, a downhill accident will occur [10]. The transmission tower accounts for about 40% of the total investment of the line, and its safety and reliability have attracted increasing attention in modern society. Therefore, it is very necessary to study and analyze the ultimate bearing capacity of transmission towers, which has important reference value for the design, operation, and disaster resistance of transmission lines.

Affected by various meteorological conditions, transmission line icing disasters occur frequently in various countries, and relevant personnel of scientific research and design units have carried out a lot of research work [11–13]. The formation of transmission line icing is a complex physical process with many influencing factors, and various meteorological conditions have a great impact on icing. However, the research on how to monitor these meteorological conditions and obtain the exact meteorological parameters is not very mature. With the in-depth study of the physical characteristics of ice cover, researchers have developed many snow cover prediction models, such as Ackley model, Lozowski model, Pots model, Chain model, Jones model, and Makkonen model. The advantages of the above model are different in different cases, but the physical parameters such as the size of water droplets and the content of liquid water are not easy to obtain.

The load of transmission tower caused by icing is divided into transverse load, longitudinal load, and vertical load according to the action direction. The transverse load is the load along the cross-arm direction, the longitudinal load is the load perpendicular to the cross-arm direction, and the vertical load is the load perpendicular to the ground direction [14]. Icing tower toppling is largely caused by the unbalanced tension between the adjacent two gears caused by uneven icing and different stages of deicing, which has been studied by many scholars. In the design process of transmission tower line system, the method of separate design of iron tower and conductor is usually adopted. At present, the research on the specific algorithm of the longitudinal unbalanced tension of the transmission tower is not mature. The common practice is to take the percentage of the maximum use tension of the conductor according to the specification for verification. The longitudinal unbalanced tension is one of the important factors that lead to the collapse of transmission towers and then threaten the safe operation of the power grid. Therefore, it is of great practical significance to accurately calculate the longitudinal unbalanced tension.

The relevant research methods of transmission tower structure bearing capacity analysis have been constantly explored, and some research results have been achieved [15–17]. The integration of artificial neural network (ANN) with other soft computing methods, such as backpropagation (BP), imperialist competitive algorithm (ICA), support vector regression (SVR), backpropagation neural network (BPNN), genetic algorithms (GA), and multilayer feed forward (MLFF) has been deeply reviewed [18–21]. As a classical neural network algorithm, BPNN has strong adaptability and fault-tolerant performance. In recent years, it has been widely used in the analysis of transmission tower line architecture [22–25]. To improve the performance accuracy, researchers employ different ANN methods to compare their effectiveness with different models [26–29]. BPNN was used to forecast the slump and compressive strength of composite geopolymers with its high precision and engineering applicability, the prediction results of BPNN were also compared with random forest (RF) and k nearest neighbors (KNN) algorithm model [30]. However, BPNN model has some problems, such as low-prediction accuracy, possible over fitting and easy to fall into local optimization [31]. Among lots of intelligence algorithms [32–35], fireworks algorithm (FWA) is a swarm intelligence algorithm inspired by fireworks explosion in the night sky, which is

mainly composed of explosion operator, mutation operation, mapping rules, and selection strategy [36–38]. A novel hybrid optimization algorithm named GPOFWA integrates political optimizer (PO) with FWA to solve numerical and engineering optimization problems [39–41]. Multimodal multiobjective optimization problems (MMOPs) have received increasing attention, which can be solved by FWA [42–45]. Furthermore, FWA has been applied in many fields since it was proposed, and has good performance in prediction accuracy and local optimization prevention [46–50].

Therefore, this paper establishes a prediction model of structural bearing capacity based on FWA by analyzing the correlation between structural bearing capacity and temperature, humidity, wind speed, terrain, altitude, condensation height, and other factors. By using the FWA to optimize the weights and thresholds of the BP neural network, the optimization ability of the neural network is further improved, which can more accurately predict the structural bearing capacity of the transmission tower line system, identify the weak parts of the transmission tower under icing conditions, and effectively avoid the failure of the transmission tower structural system, to prevent icing and tower collapse. The research has necessary reference and value for the design and reinforcement of transmission towers.

2. Data Preprocessing under Icing Condition

Among the obtained data, the main influencing factors affecting the structural bearing capacity of the transmission tower under icing are terrain, altitude, condensation height, conductor diameter, conductor suspension height, temperature, humidity, wind speed, pressure, etc. Their collection time interval is 20 min, and these data are collected by data collection equipment. Because the equipment may have errors in the process of data collection and transmission, there are incomplete and abnormal data in the massive original data. The abnormality of historical data will have a great impact on the prediction effect of structural bearing capacity. On the one hand, the training of neural network depends on historical data, and the inaccuracy of data will interfere with the correct training of neural network model on the law of structural bearing capacity, resulting in poor training effect and inaccurate prediction accuracy; moreover, taking the abnormal data as the actual value of the prediction result of the verification neural network model will cause the wrong estimation of the prediction result, so it is necessary to preprocess the data and make it suitable for specific mining algorithms.

2.1. Sample Abnormal Value Handling. Outliers refer to individual values in the sample, whose values deviate significantly from the rest of the observed values. The data of structural bearing capacity and meteorological factors obey normal distribution, so 3σ is selected in this paper. In principle, abnormal value detection shall be carried out. According to the definition of normal distribution, the average distance is 3σ. The probability outside is $P(|X-\mu|>3\sigma) \leq 0.003$, which is a minimum probability event. By default, it can be determined that the distance exceeds the average value by 3σ. The sample of does not exist, so if the difference between the observed value and the average value exceeds three times the standard deviation, it can be regarded as an abnormal value. After detecting the abnormal value, it is necessary to select the appropriate alternative value to replace the abnormal value according to some selection criteria. Analyzing the structural bearing capacity data and meteorological data, the structural bearing capacity data at each time point has its role, so the deletion method is not suitable. In this paper, the KNN method of interpolation method is used to complete the outliers. In a given data sample, the algorithm obtains the average value of the k data according to the data of the KNN near the abnormal value, and then fills the average value into the abnormal value. The algorithm is shown in Formula (1).

$$X_i = \frac{x_{i-k} + \cdots + x_{i-1} + x_{i+1} + \cdots + x_{i+k}}{2k}, \tag{1}$$

where x_{i-k} is the kth data before the outlier, and x_{i+k} is the kth data after the outlier.

2.2. Normalization of Measured Data for Transmission Tower. Different evaluation indicators often have different dimensions and dimensional units, which will affect the results of data analysis. In order to eliminate the dimensional impact between indicators, data standardization is needed to solve the comparability between data indicators. Among them, the most typical is data normalization. The units of structural bearing capacity and meteorological environment data are different, and the values are also different. Taking them directly as the input data of structural bearing capacity prediction model will affect the prediction accuracy and cannot guarantee the effectiveness of experimental results. The ANN uses nonlinear activation function, and its output is limited to $[0, 1]$ or $[-1, 1]$. In order to prevent neuron saturation caused by the use of original data, it is also necessary to normalize the data, and uniformly scale the data of multiple variables to the range of $[0, 1]$. The model uses Formula (2) to standardize the data.

$$x^* = \frac{x - \min}{\max - \min}, \tag{2}$$

where max is the maximum value of the original sequence data, min is the minimum value of the original sequence data, x is the value of the current point, and x^* is the value calculated by the normalization conversion.

After the data is trained by neural network, the output data of neural network is still within the range of $[0, 1]$. At this time, it is also necessary to conduct inverse normalization processing on the output data to make it become dimensional data again. The inverse normalization formula is shown in Formula (3).

$$y' = y \times (\max - \min) + \min, \tag{3}$$

where y represents the output sequence data of the neural network, max and min represent the maximum and

minimum values of the original sequence data, respectively, and y' represents the data after inverse normalization.

The data standardization of all input data features eliminates the impact of different dimensions on the accuracy of the prediction model, which is conducive to accelerating the convergence speed of the model and improving the accuracy of the model.

2.3. Correlation Analysis of Influencing Factors. Correlation analysis refers to the analysis of two or more variable elements with correlation, so as to measure the correlation degree of two variable factors. Pearson product moment correlation coefficient is most commonly used to measure the relationship between two variables. Pearson correlation coefficient calculation formula is as follows:

$$r = \frac{\sum_{i=1}^{N}(X_i - \overline{X})(Y_i - \overline{Y})}{\sqrt{\sum_{i=1}^{N}(X_i - \overline{X})^2}\sqrt{\sum_{i=1}^{N}(Y_i - \overline{Y})^2}}. \quad (4)$$

(i) If $r > 0$, it indicates that there is a positive correlation between the two variables, that is, when the value of one variable increases, the value of the other variable will also increase;

(ii) If $r < 0$, it indicates that there is a negative correlation between the two variables, that is, when the value of one variable increases, the value of the other variable decreases;

(iii) If $r = 0$, it indicates that there is no linear correlation between the two variables.

In addition, the absolute value of r reflects the strength of correlation, many factors affect the structural bearing, and there is coupling between them. If all the influencing factors are considered in the actual structural bearing capacity prediction, it will increase the difficulty of structural bearing capacity prediction. Therefore, Pearson correlation coefficient is used to analyze the correlation between the structural bearing capacity data and various influencing factors. The correlation analysis results are shown in Table 1.

It can be seen from Table 1 that among the various factors affecting the bearing capacity of the structure, the correlation coefficient of temperature is the highest, while the correlation coefficient of load current is the lowest. The first five characteristic variables (temperature, humidity, member load, wind speed, and geographical height) with the highest correlation coefficient are selected as the input variables of the next algorithm model. Through screening, the number of features is reduced, which helps to reduce the calculation time and cost. Hence, selecting features with higher correlation coefficient is also conducive to improving the accuracy of power prediction model.

Table 1: Correlation analysis results of structural bearing capacity and influencing factors under icing.

No.	Influence factor	Correlation coefficient
1	Temperature	−0.852
2	Humidity	0.836
3	Member load	0.728
4	Condensation height	0.471
5	Conductor suspension height	0.393
6	Wire diameter	0.284
7	Wind speed	0.842
8	Load current	0.279
9	Geographical height	0.823

3. Improved Algorithm Model

BPNN generally refers to a multilayer feed forward neural network trained by error back propagation calculation theory. Neural network has the ability of self-learning, self-adaptive, and high-speed search for optimal solutions. It does not need to establish complex mathematical and physical models, but only needs to provide historical data, and can get better prediction results. Therefore, it is widely used in the field of prediction. The process of FWA generating normal Mars provides the algorithm with search ability, and the process of generating special Mars and selection process provide the algorithm with the ability to jump out of local optimization. Because the icing bearing capacity of transmission tower is a nonstationary random process, the initial value of BPNN training is irregular. Using FWA to optimize the initial weight and threshold of BPNN can make BPNN better train and predict the data.

3.1. Setting of BPNN. Input layer, hidden layer, and output layer are the basic structure of BPNN. The input variables of BPNN are the temperature, humidity, member load, wind speed, and altitude of the 2 days before the prediction day, and the structural bearing capacity of the prediction day, that is, the numbers of input nodes and output nodes of BPNN are 5 and 2, which is to predict the axial stress of transmission tower members and maximum displacement between member nodes of the transmission tower on that day. For the determination of the number of hidden layer nodes, first, the range of hidden layer nodes is obtained through empirical Formula (5), and then after repeated tests, the number of hidden layer nodes is set to 6.

$$s = \sqrt{m + n} + a, \quad (5)$$

where m and n represent the number of input layer nodes and output layer nodes of the neural network, respectively, and a is a constant between 0 and 10.

In the prediction model of neural network, sigmoid function is used for the activation function of input layer and output layer, and gradient descent method is mainly used for the training of neural network.

Network learning rate is one of the key parameters of neural network. The lower the learning rate is, the slower the change speed of loss function is, the longer the convergence time is, and it is easy to fall into local optimization. The learning rate is too large, which can accelerate the learning

Table 2: Key parameters of BP neural network.

Parameter	Parameter description	Parameter value
Lr	Learning rate	0.02
Mc	Momentum factor	0.09
Epochs	Training maximum iterated algebra	300
Goal	Minimum error of training target	0.001

in the early stage of algorithm optimization, making the model easier to approach the local or global optimal solution, but there will be large fluctuations in the later stage, and even the value of the loss function will hover around the optimal solution. Momentum factor is mainly to accelerate the convergence speed of the network. The selection of network learning rate and momentum factor in this study is debugged many times. The number of iterations mainly takes into account the running time and whether the network is fully iterated and updated. Too much iteration will lead to too long running time, too little iteration, and fast running will lead to insufficient iterations. The network still has room for optimization. The number of iterations is generally 100–500, depending on the operation. The details of parameter settings are shown in Table 2.

3.2. Improved Fireworks Algorithm. In order to realize the global and local ergodic search of FWA for the optimal value of the explosion, the explosion amplitude identification influence factor e is introduced into the explosion radius of the FWA, as shown in Formula 6.

$$R_i' = \left| r - (R_{\max} - R_{\min}) \times \frac{g}{T} \times e \right|, \tag{6}$$

where R_i' adopts the amplitude linear decreasing strategy, which can realize both global search and local fine traversal search; $R_{\min} < r \leq R_{\max}$, r is a constant, which is used to control the explosion amplitude of fireworks. $R_{\max}$ and $R_{\min}$ are the maximum and minimum explosion amplitude of fireworks, respectively; g is the current iteration number, and T is the total number of iterations; $e = f_{\text{zbest}} + f_{\text{bad}} - f(X_i) + \varepsilon / f(X_i) + \varepsilon$, f_{zbest} is the current global optimal fitness, and f_{bad} is the current global worst fitness. When $f(X_i) = f_{\text{zbest}}$, $e = f_{\text{bad}}/f_{\text{zbest}} > 1$, then the f_{itness} value is the best, the search radius is the smallest, and local fine search is carried out; when $f(X_i) = f_{\text{bad}}$, $e = f_{\text{zbest}}/f_{\text{bad}} < 1$, the fitness value is the worst, the search radius is the largest, and the global search is a better value; When $f(X_i)$ is other values, $f_{\text{zbest}}/f(X_i) \leq e \leq f_{\text{bad}}/f(X_i)$, the optimization is carried out in a linear decreasing manner from global to local with the increase of the current iteration number g. When the explosion search radius is from outside to inside, from $R_{\max}$ (or r) to $R_{\min}$ (or 0), the global search is realized. When the search radius is from inside to outside, from $R_{\min}$ (or 0) to R or the fine search is carried out near the explosion point, because there are more high-quality sparks near the explosion point, this can ensure the fine search near the explosion point. The original explosion search takes the fitness value as the radius and expands the search one by one. The search efficiency is low and it is easy to fall into local optimization. The improved explosion amplitude gradually shrinks with the increase of the current iteration times, and the search efficiency is greatly improved. The factor e can reflect the search radius, which can not only achieve high-efficiency global search, but also achieve local fine search, especially strengthen the search near the origin.

Table 3: Key parameter selection of improved fireworks algorithm.

Parameter	Parameter description	Parameter value
D	Size of firework population	5
M	Firework explosion spark number adjustment constant	8
L_m	Upper bound of the number of firework explosion sparks	5
B_m	Lower bound of the number of firework explosion sparks	1
G	Gaussian variation spark number	5
T	Maximum iterated algebra	300

According to the steps of the FWA, the key parameters are set as follows: the population size determines the diversity of sparks. The population size is generally selected as five, and the number of sparks determines the number of sparks generated by explosion. The more the number, the greater the possibility of finding the optimal solution, but the longer the time is required. In order to reduce the running time, the value of spark number is smaller; the upper and lower limits of sparks are used to limit the number of sparks, so that each spark can explode a new number of sparks, and its value is related to the spark adjustment constant. The variation spark number is mainly used to enhance the ability of global exploration, and the number of iterations is 100–500 generally. If the number of iterations is large, the running speed is slow. The number of iterations in this paper is set to 300. The specific parameter settings are shown in Table 3.

3.3. Improved FWA-BPNN Model. BP neural network has two obvious shortcomings: one is easy to fall into local minimum, the other is slow convergence. FWA has the advantages of simple mechanism and strong optimization ability. In the paper, FWA is introduced into neural network model to optimize the weight and threshold of neural network to achieve the most effective learning and prediction of neural network. The algorithm flow of optimizing BPNN based on FWA is shown in Figure 1, and the architecture of proposed network model is presented in Figure 2.

3.4. Validation of the Improved Model. To verify the optimization ability and effectiveness of the algorithm in this paper, three benchmark functions are used for simulation test.

$$f_1(x) = \sum_{i=1}^{D} x_i^2, \tag{7}$$

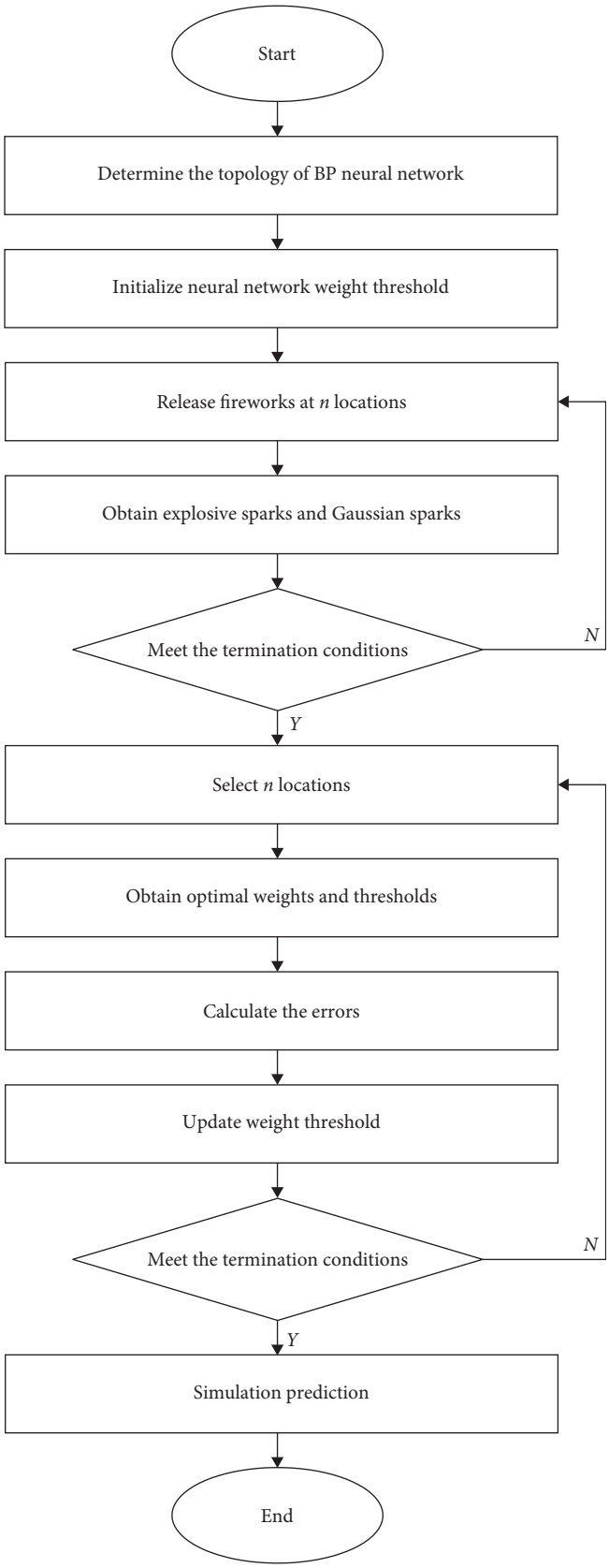

Figure 1: The flow diagram of the improved FWA-BPNN.

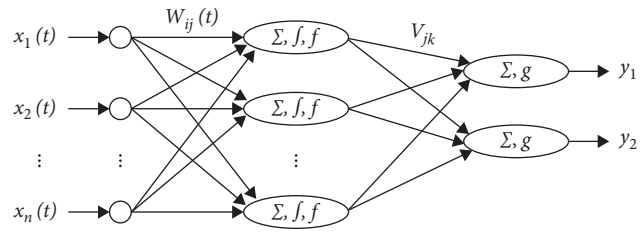

Figure 2: The architecture of proposed network model.

$$f_2(x) = -20\exp\left(-0.2\sqrt{\frac{1}{D}\sum_{i=1}^{D}x_i^2}\right) - \exp\left(\frac{1}{D}\sum_{i=1}^{D}\cos(2\pi x_i)\right), \tag{8}$$

$$f_3(x) = \sum_{i=1}^{D}(x_i^2 - 10\cos(2\pi x_i) + 10). \tag{9}$$

To further verify the prediction performance based on FWA-BPNN, the same data sets are used to train the traditional BPNN, GA improved BPNN (GA-BPNN) and particle swarm optimization algorithm improved BPNN (PSO-BPNN). The parameter setting of the GA algorithm is: population size $popu = 30$, genetic algebra $gen = 100$, crossover probability $pcross = 0.8$, and mutation probability $pmutation = 0.05$. For PSO algorithm, the parameters are: speed update parameter $c_1 = c_2 = 1.49445$, evolution times $maxgen = 150$, population size $sizepop = 30$, individual maximum $pop_{\max} = 7$, individual minimum $pop_{\min} = -7$, individual maximum speed $v_{\max} = 1$, and individual minimum speed $v_{\min} = -1$. The parameters of BPNN in BPNN prediction model optimized by different algorithms are the same as those in FWA-BPNN model. The experimental results are shown in Table 4.

From the above experiments, it can be seen that in the optimization of the three test functions, the improved FWA proposed in this paper is superior to other algorithms in accuracy, running time, stability, and convergence speed. Therefore, the FWA is very successful for the optimization of BPNN, and the optimized model is more suitable for engineering analysis and calculation.

3.5. Experimental Example Verification. In order to further verify the prediction performance of the FWA-BPNN model in the bearing capacity prediction of transmission towers, under the conditions of selecting the same training parameters and using the same dataset, the BPNN, FWA, FWA-BPNN, PSO-BPNN, and GA-BPNN prediction models for the bearing capacity of icing structures are trained and tested, respectively. When measuring the performance of the model, the following four error indicators are usually selected: root-mean-square error (RMSE), mean absolute error (MAE), and mean absolute percentage error (MAPE). RMSE accumulates the squares of errors first and then deduces the squares, which is sensitive to outliers. MAE is a basic index to investigate the average of absolute errors, and reflects the real errors. MAPE not only considers

Table 4: Comparison of optimization results of three benchmark functions by each algorithm.

Benchmark function	Algorithm name	Mean value	Standard deviation	Optimization time (s)
f_1	BP NN	1.7281×10^{-12}	5.6198×10^{-13}	48.5694
	FWA	3.1572×10^{-17}	9.3641×10^{-18}	50.0481
	GA-BP NN	0.0024	0.0138	47.8787
	PSO-BP NN	4.5293×10^{-7}	4.4127×10^{-7}	49.5428
	FWA-BPNN	2.4031×10^{-41}	8.9402×10^{-42}	41.4849
f_2	BP NN	1.5295×10^{-6}	1.1327×10^{-7}	48.5752
	FWA	1.3026×10^{-5}	1.2084×10^{-6}	55.2036
	GA-BP NN	0.0071	0.0025	64.0014
	PSO-BP NN	0.0094	0.0026	48.8123
	FWA-BPNN	8.9563×10^{-16}	0	45.9563
f_3	BP NN	4.5948×10^{-10}	9.8526×10^{-11}	48.2761
	FWA	2.6798×10^{-11}	5.5296×10^{-12}	48.5982
	GA-BP NN	0.0044	0.0003	49.1628
	PSO-BP NN	16.5288	3.3219	46.3562
	FWA-BPNN	0	0	39.6229

Table 5: Comparison of model prediction error indicators.

Index	BP NN	FWA	GA-BP NN	PSO-BP NN	FWA-BPNN
RMSE	0.83	0.76	0.74	0.71	0.59
MAE	0.65	0.64	0.59	0.58	0.53
MAPE/%	119.21	118.35	33.87	31.94	6.18
Training error	0.0128	0.0126	0.0124	0.0123	0.0130
Test error	0.0149	0.0147	0.0158	0.0145	0.0134

the error between the predicted value and the real value, but also shows the ratio of the error to the real value.

Assume that the predicted value is $x = \{x_1, x_2, \ldots, x_n\}$, and the true value is $y = \{y_1, y_2, \ldots, y_n\}$. The calculation formulas for the four indicators are as follow:

$$\mathrm{RMSE} = \sqrt{\frac{1}{n}\sum_{i=1}^{n}(x_i - y_i)^2}, \tag{10}$$

$$\mathrm{MAE} = \frac{1}{n}\sum_{i=1}^{n}|x_i - y_i|^2, \tag{11}$$

$$\mathrm{MAPE} = \frac{100\%}{n}\sum_{i=1}^{n}\left|\frac{x_i - y_i}{y_i}\right|. \tag{12}$$

In addition to the indicators of the above three evaluation models, training error and test error are also used as indicators for model evaluation. The training error is the average error of the model in the training set, which is used to measure the fitting of the model to the training set. Large training error indicates insufficient learning of training set characteristics, while too small training set indicates over learning of training set characteristics and easy over fitting. The test error is the average error of the model on the test set, which is used to measure the generalization ability of the model.

In this section, the measured data of power transmission tower monitoring over the years are used, and the 2019 annual data are intercepted for analysis. The dataset includes the temperature, humidity, member load, wind speed, geographical height, and the historical bearing capacity of the corresponding transmission tower every 15 min. Select the first 80% of the dataset as the training dataset to train the prediction model, and the last 20% of the data are set as the test data to test and verify the model. The experiment results are listed in Table 5.

From the above experiments, it can be seen from Table 5 that although the errors of different models for the prediction results of the bearing capacity of the transmission tower structure fluctuate, the error fluctuation of the prediction model based on the FWA-BPNN is smallest, and the error fluctuation of the traditional BPNN model and the traditional FWA model is large. The GA-BPNN model and the PSO-BPNN model have higher accuracy for bearing capacity prediction than the traditional BPNN model and the traditional FWA model, and are lower than the FWA-BPNN prediction model. Hence, the FWA-BPNN model proposed in this paper can be applied to the structural analysis of transmission towers under icing conditions.

4. Axial Stress and Maximum Displacement Prediction Calculation Based on FWA-BPNN Prediction Model

4.1. Research Object of the Transmission Tower. 500 kV straight-line cathead tower is common in southwest, northwest, and central of China. The main material of the transmission tower is Q345 steel, and the inclined material and

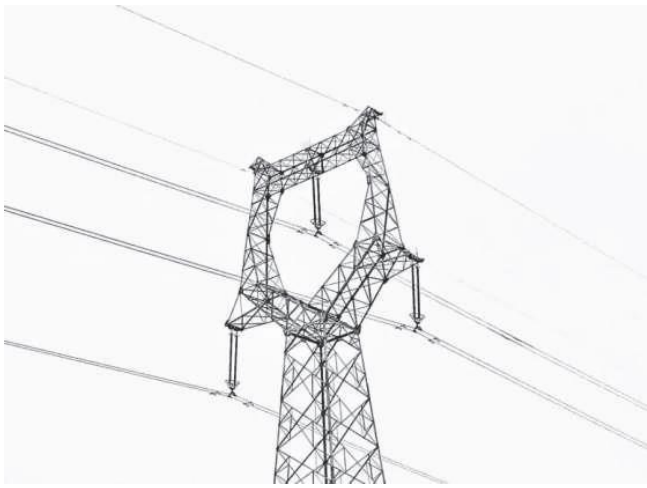

Figure 3: Schematic of the transmission tower.

auxiliary material are Q235 steel, which is within 1,000 m above sea level. The design wind speed is 30 m/s, and the conductor is 4 × LGJ-400/35 single circuit iron tower. The nominal height of the transmission tower is 48 m, the horizontal span is 500 m, the vertical span is 700 m, and the representative span is 400 m. In the southwest and central of China, the average temperature is almost higher than 0°C, but affected by the Siberian cold current and the warm and humid climate of the Pacific Ocean, short-term rime and rime icing meteorological conditions occur almost every winter. The average number of rime days is 3–15 days. The short-term rime icing has caused huge losses to the power system. The structural diagram of the transmission tower is given in Figures 3–6.

4.2. Structural Bearing Capacity Analysis of Transmission Tower Steel Members Based on Improved FWA-BPNN Model. Using the BP neural network model optimized by the FWA proposed in this paper, the axial stress of tower members and maximum displacement between member nodes of the transmission tower under the icing condition calculations are carried out for this transmission tower, and the node number of the rod starts from the top left. Some calculation results are listed in Tables 6–10, and P_d is the design load in the tables.

By analyzing the failure member load stress in Tables 6–10 of the above transmission tower under icing conditions, it can be seen that under the design load, four inclined beams above the transverse septum of the neck were damaged. Supposing the load step is $1.14P_d$, the failure bars of the transmission tower spread to the symmetrical sides of the tower top and tower head, respectively. Once the load step is $1.28P_d$, the failure part does not spread, but when the load is $1.44P_d$, the number of failed members continues to increase. As the load step is $1.61P_d$, the tensile strength of two inclined materials on the leeward side of the middle of the tower head is damaged. When the load step is $1.79P_d$, two damaged inclined materials are added on one side of the cross arm of the middle conductor. If the load step is $1.98P_d$, the damaged inclined material spreads to the other side of the middle conductor cross arm, and the tensile strength of two inclined materials

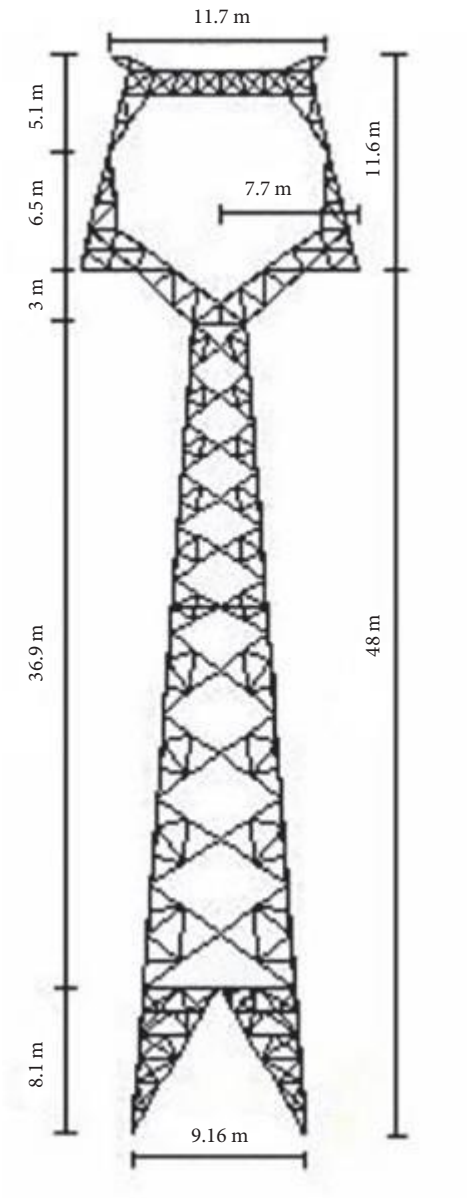

Figure 4: Vertical view of transmission tower (along the line).

on the windward side in the middle of the tower head is damaged. When the load is $2.18P_d$, two damaged diagonal members are added above the cross arm of the middle conductor, and at the same time, the number of damaged diagonal members above the neck diaphragm is increased. Once the load is $2.40P_d$, the number of damaged diagonal members above the neck diaphragm continues to increase. When the load is $2.62P_d$, the number of failed members continues to increase. If the load is $3.11P_d$, two damaged diagonal members are added under the cross arm of the middle conductor. When the load is $3.50P_d$, the main material above the middle conductor cross arm is damaged, the tensile strength of two main materials below the middle conductor cross arm is damaged, the main material on the neck diaphragm is damaged, and the main material above the neck diaphragm is damaged. If the ice thickness reaches 36 mm, the overall stiffness matrix of

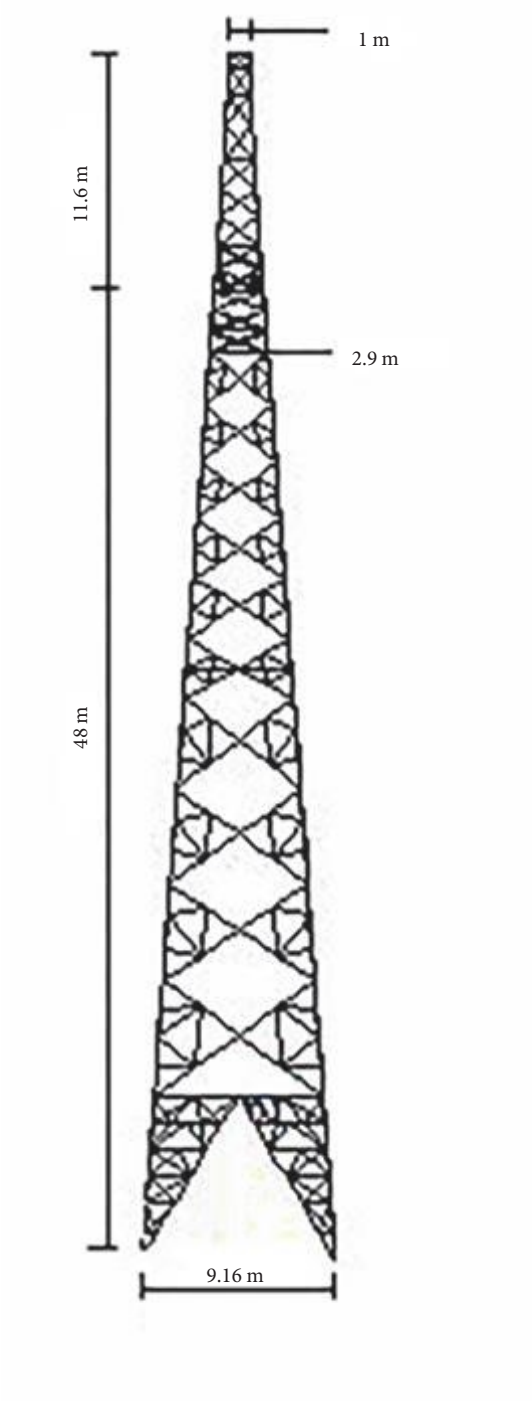

Figure 5: Transverse elevation of transmission tower.

the structure is singular, and the program exits, and the transmission tower structure reaches the ultimate bearing capacity.

5. Conclusions

(i) In order to ensure the stability of the mechanical structure of the transmission tower and further improve the accuracy of bearing capacity prediction, this paper proposes a BP neural network prediction model based on FWA optimization. Through data processing and algorithm model experimental analysis, it shows that through the calculation and analysis of data normalization and correlation, the dimension of the data is reduced, thus reducing the calculation cost, and making relevant preparations for improving the accuracy of the model in the later stage.

(ii) For the sake of realizing the global and local ergodic search for the optimal value of the explosion, the explosion amplitude judgment factor e is introduced into the explosion radius of FWA, which greatly improves the search efficiency. By introducing FWA to optimize the weight and threshold of BP neural network, the shortcomings of BP neural network easy to fall into the minimum and slow convergence speed are solved, and the prediction accuracy is improved.

(iii) The experiment compares FWA-BPNN model with traditional BP neural network and other neural network models. The results show that the prediction

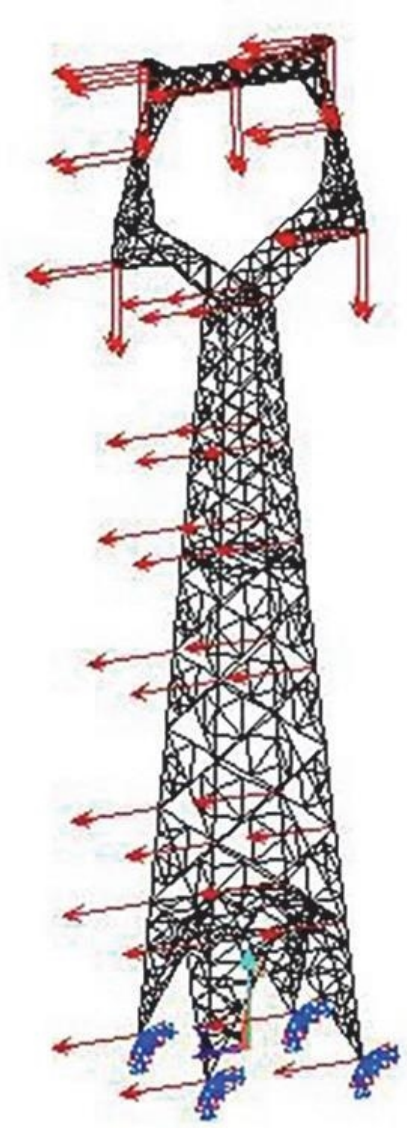

Figure 6: Load diagram of transmission tower under icing condition.

Table 6: Transmission tower member stress list (I).

Member no.	$1.00P_d$		$1.14P_d$		$1.28P_d$	
	Failure stress (MPa)	Actual stress (MPa)	Failure stress (MPa)	Actual stress (MPa)	Failure stress (MPa)	Actual stress (MPa)
258	−143.53	−47.73	−143.43	−54.12	−144.53	−56.99
260	−144.54	46.57	−144.21	53.41	−144.65	60.77
270	292.78	108.47	292.85	119.66	292.67	134.11
275	294.01	104.03	294.05	115.32	294.67	126.03
289	−138.96	−54.18	−138.75	−59.12	−140.03	−65.56
296	−154.98	59.16	−155.77	65.30	−155.98	73.07
297	−155.86	55.04	−154.86	61.10	−157.01	68.01
678	−126.43	31.01	−126.46	33.98	−126.01	38.77
685	−197.48	74.91	−199.02	83.00	−200.04	90.88
1,147	−60.04	−25.14	−60.12	−28.11	−60.04	−29.46
1,161	−49.63	−7.03	−49.02	−7.04	−49.01	−7.98
1,163	200.35	120.14	200.15	133.22	200.43	145.67
1,164	−109.12	−109.01	−109.12	−119.67	−109.23	
1,165	−104.52	−74.07	−104.57	−82.05	−104.05	−91.13
1,166	−64.65	−56.95	−64.14	−63.01	−64.56	−69.12
1,168	−65.06	−74.15	−64.11		−64.99	
1,170	−74.37	−56.97	−74.77	−63.32	−74.56	−69.33
1,172	−76.85	−74.67	−76.68	−81.30	−76.78	
1,175	−105.41	−74.17	−104.37	−82.02	−104.09	−91.08
1,176	200.43	120.02	200.15	133.04	200.65	145.98
1,177	−130.01	−107.57	−127.98	−119.82	−127.89	−133.33
1,198	−84.14	−33.44	−84.32	−36.72	−84.32	−39.12
1,199	−83.98	−33.08	−84.64	−36.60	−84.09	−39.06
1,202	−84.15	−44.13	−84.17	−49.03	−84.25	−54.34
1,203	−84.18	−44.39	−84.18	−49.53	−84.15	−54.61
1,224	−141. 73	−81.92	−141.17	−91.17	−141.75	−99.89
1,235	−149.98	−81.96	−149.77	−91.27	−149.98	−100.09
1,337	−115.98	−110.02	−116.05	−122.41	−116.07	
1,338	200.05	143.03	200.61	158.13	200.43	171.99
1,339	−105.50	−89.51	−105.51	−98.54	−105.65	−108.10
1,342	−89.16	−92.02	−89.14		−89.16	
1,348	−89.14	−91.98	−89.16		−89.16	
1,350	−67.22	−73.09	−67.35		−67.54	
1,351	−104.97	−89.15	−104.93	−98.51	−104.99	−108.13
1,352	−118.14	−110.09	−118.11	−123.23	−118.16	
1,353	199.98	142.11	200.05	157.23	199.97	173.14
1,355	−49.42	−8. 55	−48.99	−9. 37	−49.51	−9.79
1,389	−70.04	−25.02	−70.15	−28.54	−70.14	−32.04
1,419	−119.61	−74.56	−119.59	−82.31	−119.60	−90.12
1,430	−119.59	−74.51	−119.60	−82.28	−119.58	−90.23
1,443	−114.53	−45.26	−114.61	−50.19	−114.52	−55.26
1,444	−126.57	−60.50	−126.60	−66.80	−126.59	−73.70
1,455	−84.88	−44.14	−84.98	−48.86	−85.18	−53.87
1,456	−85.01	−44.21	−84.99	−48.90	−85.03	−53.79
1,458	−84.96	−33.28	−84.89	−36.76	−85.05	−40.67
1,467	−65.03	−25.22	−64.97	−28.10	−65.06	−30.98
1,472	−49.92	−18.71	−49.99	−20.05	−50.02	−22.89
1,487	−49.98	−22.69	−50.02	−25.16	−50.04	−27.75
1,492	−44.78	−20.99	−44.91	−23.15	−44.89	−25.17

Table 7: Transmission tower member stress list (II).

Member no.	$1.44P_d$		$1.61P_d$		$1.79P_d$	
	Failure stress (MPa)	Actual stress (MPa)	Failure stress (MPa)	Actual stress (MPa)	Failure stress (MPa)	Actual stress (MPa)
258	−146.26	−65.64	−144.44	−69.35	−146.27	−76.98
260	−146.67	64.36	−144.74	73.35	−147.74	80.09
270	294.27	145.64	295.26	164.53	295.74	175.66
275	295.52	140.46	294.86	155.53	294.85	166.63
289	−140.52	−73.66	−140.96	−80.35	−140.58	−86.03
296	−155.52	79.35	−155.86	85.35	−155.99	95.56
297	−155.25	72.53	−155.59	82.53	−155.96	90.63
678	−125.25	43.97	−126.75	45.35	−127.69	53.66
685	−200.11	99.64	−200.77	113.53	−200.69	123.55
1,147	−60.53	−34.64	−60.57	−37.53	−59.69	−44.55
1,161	−49.53	−7.14	−49.75	−8.09	−50.69	−8.64
1,163	200.74	165.60	200.55	179.85	200.69	196.66
1,164	−109.47		−109.85		−109.96	
1,165	−105.75	−100.46	−105.77	−109.70	−105.56	
1,166	−64.77		−65.77		−65.35	
1,168	−64.56		−66.57		−64.53	
1,170	−74.27	−77.64	−74.46		−74.53	
1,172	−76.85		−76.56		−76.53	
1,175	−105.86	−99.86	−105.67	−111.86	−104.47	
1,176	200.85	165.64	200.76	180.86	200.55	194.66
1,177	−127.78		−130.68		−128.57	
1,198	−84.25	−45.86	−84.56	−47.97	−84.55	−52.55
1,199	−83.63	−44.44	−84.54	−48.46	−83.57	−53.03
1,202	−84.53	−60.64	−83.64	−65.64	−84.75	−73.55
1,203	−84.15	−59.01	−84.28	−63.17	−84.28	−67.31
1,224	−141.73	−111.09	−141.74	−121.15	−141.56	−133.03
1,235	−149.69	−109.86	−149.68	−119.79	−149.66	−131.90
1,337	−116.05		−116.03		−116.07	
1,338	200.55	190.05	200.63	207.31	200.61	
1,339	−105.57		−105.48		−105.63	
1,342	−89.16		−89.14		−89.17	
1,348	−89.15		−89.16		−89.16	
1,350	−67.59		−67.46		−67.55	
1,351	−105.01		−104.97		−104.99	
1,352	−118.16		−118.21		−118.14	
1,353	199.95	190.03	200.01	207.45	200.05	
1,355	−48.99	−10.16	−49.32	−11.73	−49.45	−18.24
1,389	−69.97	−33.60	−70.13	−37.30	−70.15	−48.13
1,419	−119.61	−99.46	−119.57	−109.34	−119.61	−121.59
1,430	−119.57	−99.51	−119.61	−109.28	−119.60	−121.71
1,443	−114.47	−60.14	−114.51	−66.52	−114.61	−72.87
1,444	−126.59	−81.26	−126.66	−89.41	−126.78	−97.78
1,455	−85.08	−59.16	−84.98	−65.49	−85.15	−72.21
1,456	−84.96	−59.21	−84.87	−65.61	−85.06	−72.26
1,458	−84.97	−45.75	−85.05	−49.69	−84.98	−53.95
1,467	−65.03	−32.10	−64.97	−35.20	−65.03	−38.60
1,472	−49.99	−24.85	−50.02	−27.42	−49.96	−29.79
1,487	−49.95	−30.15	−49.92	−32.71	−50.04	−34.68
1,492	−44.91	−28.37	−44.87	−30.54	−44.95	−33.31

Table 8: Transmission tower member stress list (III).

Member no.	$1.98P_d$		$2.18P_d$		$2.40P_d$	
	Failure stress (MPa)	Actual stress (MPa)	Failure stress (MPa)	Actual stress (MPa)	Failure stress (MPa)	Actual stress (MPa)
258	−144.46	−85.36	−146.47	−94.85	−146.74	−101.42
260	−144.85	89.36	−146.47	100.08	−146.47	109.05
270	295.26	195.46	295.47	212.28	295.28	231.02
275	295.24	185.08	295.47	204.71	295.27	222.25
289	−140.66	−95.45	−140.84	−103.34	−140.67	−112.42
296	−155.76	106.05	−155.47	115.06	−155.73	125.05
297	−155.64	98.43	−155.74	108.76	−155.36	117.05
678	−127.64	59.66	−127.85	65.86	−127.36	70.72
685	−200.63	135.06	−200.53	145.63	−200.33	160.52
1,147	−60.42	−45.47	−60.57	−55.63	−60.36	−62.55
1,161	−49.74	−14.09	−49.75	−19.09	−49.63	−24.75
1,163	200.46	208.67	200.85		200.63	
1,164	−109.47		−109.64		−109.89	
1,165	−105.75		−105.67		−105.46	
1,166	−65.74		−64.46		−65.64	
1,168	−66.59		−66.54		−66.54	
1,170	−74.21		−74.66		−74.61	
1,172	−76.64		−76.56		−76.56	
1,175	−105.15		−105.16		−105.14	
1,176	200.65	208.75	200.76		200.64	
1,177	−130.15		−130.16		−130.46	
1,198	−84.53	−57.47	−84.56	−63.53	−85.46	−68.86
1,199	−84.35	−58.47	−84.55	−63.75	−85.56	−68.86
1,202	−84.42	−79.07	−84.42	−84.64	−84.53	−85.28
1,203	−84.28	−70.90	−84.24	−76.34	−84.28	−81.10
1,224	−141.73	−147.55	−141.71		−141.73	
1,235	−149.88	−144.97	−149.78	−157.89	−149.68	
1,337	−116.04		−116.05		−116.08	
1,338	200.55		200.74		200.69	
1,339	−105.57		−105.61		−105.63	
1,342	−89.16		−89.13		−89.17	
1,348	−89.14		−89.16		−89.15	
1,350	−67.57		−67.59		−67.61	
1,351	−105.07		−104.89		−105.03	
1,352	−118.16		−118.21		−118.13	
1,353	199.95		200.05		200.03	
1,355	−49.42	−25.14	−48.98	−32.02	−49.37	−37.34
1,389	−70.09	−58.25	−69.99	−66.69	−70.11	−74.43
1,419	−119.56		−119.60		−119.57	
1,430	−119.60		−119.58		−119.61	
1,443	−114.51	−79.80	−114.53	−87.65	−114.61	−95.90
1,444	−126.60	−107.53	−126.59	−117.71	−126.64	−129.53
1,455	−84.99	−77.90	−85.05	−87.12	−85.08	
1,456	−85.05	−77.90	−85.01	−87.10	−85.01	
1,458	−84.98	−58.60	−85.05	−65.21	−84.96	−70.10
1,467	−65.06	−44.32	−65.03	−47.54	−64.97	−51.22
1,472	−49.97	−33.17	−50.04	−34.42	−50.02	−37.31
1,487	−50.02	−38.56	−49.98	−40.23	−50.04	−42.45
1,492	−44.87	−35.18	−44.92	−38.63	−44.89	−41.49

Table 9: Transmission tower member stress list (IV).

Member no.	$2.62P_d$		$3.11P_d$		$3.50P_d$	
	Failure stress (MPa)	Actual stress (MPa)	Failure stress (MPa)	Actual stress (MPa)	Failure stress (MPa)	Actual stress (MPa)
258	−144.85	−110.24	−146.26	−133.52	−146.44	−150.16
260	−144.65	121.28	−146.67	136.19	−146.47	150.87
270	294.74	253.55	295.47	285.23	295.52	310.64
275	294.86	244.65	295.27	276.87	295.47	303.18
289	−140.52	−120.53	−140.67	−137.22	−140.85	−145.65
296	−155.76	135.11	−155.73	153.45	−155.98	168.48
297	−155.59	126.70	−155.71	144.86	−155.96	160.03
678	−126.71	79.65	−127.51	98.41	−127.89	136.85
685	−200.53	176.34	−200.75	193.51	−200.81	196.62
1,147	−60.45		−60.51		−60.57	
1,161	−49.79	−32.56	−50.32	−55.95	−49.72	
1,163	200.43		200.63		200.75	
1,164	−109.81		−109.75		−109.85	
1,165	−105.45		−105.56		−105.75	
1,166	−64.74		−64.85		−65.35	
1,168	−66.59		−66.54		−66.57	
1,170	−74.37		−74.53		−74.56	
1,172	−76.79		−76.85		−76.68	
1,175	−105.17		−105.41		−105.56	
1,176	200.15		200.65		200.64	
1,177	−130.09		−130.13		−130.18	
1,198	−84.46	−75.61	−84.58	−87.90	−84.58	
1,199	−83.98	−74.19	−84.46	−86.73	−84.54	
1,202	−84.42		−84.25		−84.53	
1,203	−84.18	87.28	−84.28		−84.24	
1,224	−141.73		−141.56		−141.75	
1,235	−149.68		−149.77		−149.78	
1,337	−116.08		−116.05		−116.07	
1,338	200.43		200.61		200.55	
1,339	−105.63		−105.57		−105.61	
1,342	−89.16		−89.18		−89.14	
1,348	−89.14		−89.16		−89.17	
1,350	−67.49		−67.31		−67.54	
1,351	−104.99		−104.97		−105.03	
1,352	−118.20		−118.13		−118.16	
1,353	200.05		199.98		200.05	
1,355	−49.92	−53.86	−48.99		−49.32	
1,389	−69.99		−70.04		−70.14	
1,419	−119.57		−119.61		−119.63	
1,430	−119.56		−119.58		−119.57	
1,443	−114.63	−105.03	−114.49	−119.31	−114.67	
1,444	−126.47		−126.60		−126.73	
1,455	−85.18		−84.89		−84.98	
1,456	−84.97		−85.01		−85.05	
1,458	−84.89	−77.35	−85.05	−87.64	−85.11	
1,467	−65.03	−55.96	−65.04	−64.42	−65.06	−72.17
1,472	−49.96	−39.34	−50.03	−55.78	−50.02	
1,487	−49.95	−53.51	−49.92		−50.04	
1,492	−44.92	−46.67	−44.82		−44.79	

Table 10: Displacement under different icing thickness.

Icing thickness (mm)	Displacement in X direction (mm)	Displacement in Y direction (mm)	Displacement in Z direction (mm)	Total displacement (mm)
10	≤0.001	65.25	−15.77	67.23
10.5	≤0.001	65.89	−16.57	68.33
11	≤0.001	66.54	−17.24	69.86
11.5	≤0.001	68.01	−18.03	70.72
12	≤0.001	69.85	−18.85	72.47
12.5	≤0.001	70.11	−19.11	73.56
13	≤0.001	71.27	−19.53	74.08
13.5	≤0.001	73.01	−19.89	75.63
14	≤0.001	74.42	−20.84	77.05
14.5	≤0.001	75.32	−20.91	78.65
15	≤0.001	76.35	−21.14	80.57
15.5	≤0.001	77.97	−22.57	81.38
16	≤0.001	79.04	−23.67	82.33
16.5	≤0.001	80.47	−24.02	83.45
17	≤0.001	81.95	−24.24	85.36
17.5	≤0.001	82.11	−25.36	86.73
18	≤0.001	83.55	−26.18	88.95
18.5	≤0.001	84.98	−26.79	89.55
19	≤0.001	86.25	−27.15	91.36
19.5	≤0.001	88.04	−28.43	92.58
20	≤0.001	89.52	−29.89	94.37
20.5	≤0.001	90.85	−30.07	95.35
21	≤0.001	92.95	−30.36	97.85
21.5	≤0.001	94.12	−31.43	99.17
22	≤0.001	95.73	−32.96	101.36
22.5	≤0.001	97.04	−34.16	103.44
23	≤0.001	98.55	−35.04	105.07
23.5	≤0.001	99.56	−36.55	106.72
24	≤0.001	100.35	−38.53	108.40
24.5	≤0.001	101.51	−40.74	111.06
25	≤0.001	103.91	−43.07	113.74
25.5	≤0.001	104.79	−45.32	114.79
26	≤0.001	106.25	−47.33	116.34
26.5	≤0.001	107.31	−48.83	118.44
27	≤0.001	108.75	−51.28	120.47
27.5	≤0.001	109.52	−53.55	123.54
28	≤0.001	111.54	−55.26	125.57
28.5	≤0.001	113.64	−57.33	129.05
29	≤0.001	115.12	−60.47	131.55
29.5	≤0.001	117.42	−62.55	134.25
30	≤0.001	120.74	−64.56	137.93
30.5	≤0.001	122.76	−68.32	141.68
31	≤0.001	125.53	−70.07	145.46
31.5	≤0.001	128.33	−72.69	149.27
32	≤0.001	131.63	−75.36	152.68
32.5	≤0.001	134.78	78.23	157.59
33	≤0.001	137.75	−81.96	160.75
33.5	≤0.001	140.03	−85.24	163.98
34	≤0.001	142.53	−88.78	168.05
34.5	≤0.001	145.51	91.49	173.66
35	≤0.001	148.69	−95.44	177.90

result of FWA-BP neural network is closer to the actual value, the error is smaller, and the model is more stable. The improved FWA-BP neural network is applied to the structural bearing capacity analysis of transmission tower line under icing, which realizes the accurate prediction of bearing capacity under complex meteorological conditions, and provides a reference for the study of transmission tower engineering mechanics.

By using the FWA to analyze the ultimate bearing capacity and study the failure path of the 500 kV linear cathead tower structure, the weak parts of the transmission tower under icing conditions are accurately identified. Obviously, this method can effectively predict the damage of the transmission tower structure and the results are highly reliable. In the future, further in-depth research will be conducted on the damage prediction of transmission tower structures under different transmission tower types, voltage levels, and design conditions.

Data Availability

The data used to support the findings of this study are included within the article.

Conflicts of Interest

The authors declare that they have no conflicts of interest.

Acknowledgments

The authors appreciate the financial support from the Special Research Project of Basic Business in Colleges and Universities [grant no. 135509212 and 145209147]; and Provincial Platform Opening Project of Heilongjiang Province of China [grant no. WNCGQJKF202101] and acknowledge the technical support from the transmission tower design and construction enterprises for this work.

References

[1] N. Wen, B. Yan, Z. Y. Mou, G. Z. Huang, H. X. Yang, and X. Lv, "Prediction models for dynamic response parameters of transmission lines after ice-shedding based on machine learning method," *Electric Power Systems Research*, vol. 202, Article ID 107580, 2022.

[2] X. Xie, Y. Wu, K. Liang, S. Liu, and J. Peng, "Experiment study on dynamic effects of tower-line systems induced by ice shedding," *Advances in Civil Engineering*, vol. 2020, Article ID 6241789, 9 pages, 2020.

[3] S. Alshurafa, A. Rose, and D. Polyzois, "Effects of icing, prestressing and laminate buckling stresses on the design of guyed towers," *Mechanics of Advanced Materials and Structures*, vol. 28, no. 21, pp. 2229–2241, 2021.

[4] K. Ji, X. Rui, L. Li, F. Yang, and G. McClure, "Dynamic response of iced overhead electric transmission lines following cable rupture shock and induced ice shedding," *IEEE Transactions on Power Delivery*, vol. 31, no. 5, pp. 2215–2222, 2016.

[5] X. Xu, D. Niu, P. Wang, Y. Lu, and H. Xia, "The weighted support vector machine based on hybrid swarm intelligence optimization for icing prediction of transmission line," *Mathematical Problems in Engineering*, vol. 2015, Article ID 798325, 9 pages, 2015.

[6] K. Ji, X. Rui, L. Li, C. Zhou, C. Liu, and G. McClure, "The time-varying characteristics of overhead electric transmission lines considering the induced-ice-shedding effect," *Shock and Vibration*, vol. 2015, Article ID 635230, 8 pages, 2015.

[7] B. Chen, W.-H. Guo, P.-Y. Li, and W.-P. Xie, "Dynamic responses and vibration control of the transmission tower-line system: a state-of-the-art review," *The Scientific World Journal*, vol. 2014, Article ID 538457, 20 pages, 2014.

[8] H. Yang, C. Y. Chung, J. Zhao, and Z. Dong, "A probability model of ice storm damages to transmission facilities," *IEEE Transactions on Power Delivery*, vol. 28, no. 2, pp. 557–565, 2013.

[9] B. Yan, K. Chen, Y. Guo, M. Liang, and Q. Yuan, "Numerical simulation study on jump height of iced transmission lines after ice shedding," *IEEE Transactions on Power Delivery*, vol. 28, no. 1, pp. 216–225, 2013.

[10] Y. Zhou, S. J. Niu, J. J. Lü, and L. J. Zhao, "Meteorological conditions of ice accretion based on real-time observation of high voltage transmission line," *Chinese Science Bulletin*, vol. 57, pp. 812–818, 2012.

[11] X. Meng, L. Wang, L. Hou et al., "Dynamic characteristic of ice-shedding on UHV overhead transmission lines," *Cold Regions Science and Technology*, vol. 66, no. 1, pp. 44–52, 2011.

[12] G. A. Fenton and N. Sutherland, "Reliability-based transmission line design," *IEEE Transactions on Power Delivery*, vol. 26, no. 2, pp. 596–606, 2011.

[13] F. Yang, J. Yang, J. Han, and D. Fu, "Dynamic responses of transmission tower-line system under ice shedding," *International Journal of Structural Stability and Dynamics*, vol. 10, no. 3, pp. 461–481, 2010.

[14] F. Gani and F. Légeron, "Dynamic response of transmission lines guyed towers under wind loading," *Canadian Journal of Civil Engineering*, vol. 37, no. 3, pp. 450–465, 2010.

[15] Y. Cao, Y. Zandi, A. S. Agdas et al., "A review study of application of artificial intelligence in construction management and composite beams," *Steel and Composite Structures*, vol. 39, no. 6, pp. 685–700, 2021.

[16] X. Fang, H. Luo, and J. Tang, "Structural damage detection using neural network with learning rate improvement," *Computers & Structures*, vol. 83, no. 25-26, pp. 2150–2161, 2005.

[17] G. Zhang, C. Chen, Y. Zhang, H. Zhao, Y. Wang, and X. Wang, "Optimised neural network prediction of interface bond strength for GFRP tendon reinforced cemented soil," *Geomechanics and Engineering*, vol. 28, no. 6, pp. 599–611, 2022.

[18] M. Su, H. Peng, and S.-F. Li, "Application of an interpretable artificial neural network to predict the interface strength of a near-surface mounted fiber-reinforced polymer to concrete joint," *Journal of Zhejiang University-Science A*, vol. 22, pp. 427–440, 2021.

[19] M. A. Mashrei, R. Seracino, and M. S. Rahman, "Application of artificial neural networks to predict the bond strength of FRP-to-concrete joints," *Construction and Building Materials*, vol. 40, pp. 812–821, 2013.

[20] X. Y. Gao, R. Yi, L. Q. Zhang, X. Jiang, and J. X. Li, "Analysis of transmission tower in full-scale tests," *Buildings*, vol. 12, no. 4, Article ID 389, 2022.

[21] Z.-X. Liu and X.-B. Feng, "A real-time reliable condition assessment system for 500kv transmission towers based on stress measurement," *Mathematical Problems in Engineering*, vol. 2019, Article ID 3241897, 8 pages, 2019.

[22] L. Wang, Y. Zeng, and T. Chen, "Back propagation neural network with adaptive differential evolution algorithm for time series forecasting," *Expert Systems with Applications*, vol. 42, no. 2, pp. 855–863, 2015.

[23] B. Han, F. Geng, S. Dai, G. Gan, S. Liu, and L. Yao, "Statistically optimized back-propagation neural-network model and its application for deformation monitoring and prediction of concrete-face rockfill dams," *Journal of Performance of Constructed Facilities*, vol. 34, no. 4, 2020.

[24] Z.-J. Li, G.-Y. Kan, C. Yao, Z.-Y. Liu, Q.-L. Li, and S. Yu, "Improved neural network model and its application in hydrological simulation," *Journal of Hydrologic Engineering*, vol. 19, no. 10, 2014.

[25] H. Dongmei, H. Shiqing, H. Xuhui, and Z. Xue, "Prediction of wind loads on high-rise building using a BP neural network combined with POD," *Journal of Wind Engineering and Industrial Aerodynamics*, vol. 170, pp. 1–17, 2017.

[26] Z. Yue, Y. Ding, H. Zhao, and Z. Wang, "Case study of deep learning model of temperature-induced deflection of a cable-stayed bridge driven by data knowledge," *Symmetry-Basel*, vol. 13, no. 12, Article ID 2293, 2021.

[27] F. Kuang, Z. Long, D. Kuang, X. Liu, and R. Guo, "Application of back propagation neural network to the modeling of slump and compressive strength of composite geopolymers," *Computational Materials Science*, vol. 206, Article ID 111241, 2022.

[28] G. Chen, W. Tang, S. Chen, S. Wang, and H. Cui, "Prediction of self-healing of engineered cementitious composite using machine learning approaches," *Applied Sciences*, vol. 12, no. 7, Article ID 3605, 2022.

[29] J. Luo, R. Ren, and K. Guo, "The deformation monitoring of foundation pit by back propagation neural network and genetic algorithm and its application in geotechnical engineering," *PLOS ONE*, vol. 15, no. 7, Article ID e0233398, 2020.

[30] C. Hou and X.-G. Zhou, "Strength prediction of circular CFST columns through advanced machine learning methods," *Journal of Building Engineering*, vol. 51, Article ID 104289, 2022.

[31] X. Zhang, X. Chen, and J. Li, "Improving dam seepage prediction using back-propagation neural network and genetic algorithm," *Mathematical Problems in Engineering*, vol. 2020, Article ID 1404295, 8 pages, 2020.

[32] Y. Yu, S. Liang, B. Samali et al., "Torsional capacity evaluation of RC beams using an improved bird swarm algorithm optimised 2D convolutional neural network," *Engineering Structures*, vol. 273, Article ID 115066, 2022.

[33] Y. Yu, J. Li, J. Li, Y. Xia, Z. Ding, and B. Samali, "Automated damage diagnosis of concrete jack arch beam using optimized deep stacked autoencoders and multi-sensor fusion," *Developments in the Built Environment*, vol. 14, Article ID 100128, 2023.

[34] Y. Yu, Y. Li, and J. Li, "Nonparametric modeling of magnetorheological elastomer base isolator based on artificial neural network optimized by ant colony algorithm," *Journal of Intelligent Material Systems and Structures*, vol. 26, no. 14, pp. 1789–1798, 2015.

[35] Z. Lyu, Y. Yu, B. Samali et al., "Back-propagation neural network optimized by K-fold cross-validation for prediction of torsional strength of reinforced concrete beam," *Materials*, vol. 15, no. 4, Article ID 1477, 2022.

[36] Y. Tan and Y. Zhu, "Fireworks Algorithm for Optimization," in *Advances in Swarm Intelligence*, Y. Tan, Y. Shi, and K. C. Tan, Eds., vol. 6145 of *Lecture Notes in Computer Science*, pp. 355–364, Springer, Berlin, Heidelberg, 2010.

[37] W. Wei, H. Ouyang, S. Li, X. Zhao, and D. Zou, "A modified fireworks algorithm with dynamic search interval based on closed-loop control," *Mathematics and Computers in Simulation*, vol. 200, pp. 329–360, 2022.

[38] L. Cui, X. Yang, and Y. Liu, "Research on mathematical method image classification of convolutional neural network based on firework algorithm optimization," *Wireless Communications & Mobile Computing*, vol. 2022, Article ID 8646994, 11 pages, 2022.

[39] J. Dong, H. Zou, W. Li, and M. Wang, "A hybrid greedy political optimizer with fireworks algorithm for numerical and engineering optimization problems," *Scientific Reports*, vol. 12, Article ID 13243, 2022.

[40] Y. Lu, X. Wu, L. Yao, T. Zhang, and X. Zhou, "Multi-channel data aggregation scheduling based on the chaotic firework algorithm for the battery-free wireless sensor network," *Symmetry*, vol. 14, no. 8, Article ID 1571, 2022.

[41] W. Guo and J. Guo, "Rotor transverse slots' influence on negative sequence loss and heat distribution prediction of large generators based on improved radial basis function process neural network," *Mathematical Problems in Engineering*, vol. 2022, Article ID 1865380, 19 pages, 2022.

[42] S. Han, K. Zhu, M. C. Zhou et al., "A novel multiobjective fireworks algorithm and its applications to imbalanced distance minimization problems," *IEEE/CAA Journal of Automatica Sinica*, vol. 9, no. 8, pp. 1476–1489, 2022.

[43] W. Guo, J. Guo, and F. Miao, "Application of improved process neural network based on the fireworks algorithm in the temperature-rise predictions of a large generator rotor," *Applied Sciences*, vol. 13, no. 5, Article ID 2943, 2023.

[44] B. Jiang, Y. Qin, J. Yang, H. Li, L. Wang, and J. Wang, "Web service composition optimization with the improved fireworks algorithm," *Mobile Information Systems*, vol. 2022, Article ID 4277909, 13 pages, 2022.

[45] X. Zhao, B. Shen, L. Lin, D. Liu, M. Yan, and G. Li, "Residential electricity load forecasting based on fuzzy cluster analysis and LSSVM with optimization by the fireworks algorithm," *Sustainability*, vol. 14, no. 3, Article ID 1312, 2022.

[46] J. Guo and W. Guo, "Application of BP neural network improved by fireworks algorithm on suspender damage prediction of long-span half-through arch bridge," *Shock and Vibration*, vol. 2023, Article ID 6590979, 17 pages, 2023.

[47] J. Yu, J. Guo, X. Zhang, C. Zhou, T. Xie, and X. Han, "A novel tent-levy fireworks algorithm for the UAV task allocation problem under uncertain environment," *IEEE Access*, vol. 10, pp. 102373–102385, 2022.

[48] Y. Fan, H. Wang, X. Zhao, Q. Yang, and Y. Liang, "Short-term load forecasting of distributed energy system based on kernel principal component analysis and KELM optimized by fireworks algorithm," *Applied Sciences*, vol. 11, no. 24, Article ID 12014, 2021.

[49] L. Hui, J. Yu, A. Zhao, F. Wang, X. Yang, and M. Zhou, "Research on multi-heat-source scheduling strategy of heating system based on improved fireworks algorithm," *Energy Reports*, vol. 7, pp. 7628–7639, 2021.

[50] J. Quan and L. Shang, "An ensemble model of wind speed forecasting based on variational mode decomposition and bare-bones fireworks algorithm," *Mathematical Problems in Engineering*, vol. 2021, Article ID 6632390, 16 pages, 2021.